Detection of Multimodal Fringes for Self-Mixing-Based Vibration Measurement

Muhammad Usman, Usman Zabit, Olivier Bernal, Gulistan Raja, Thierry Bosch

Detection of Multi-Modal Fringes for Self-Mixing based Vibration Measurement

Muhammad Usman, Usman Zabit, *Member*, *IEEE*, Olivier D. Bernal, *Member*, *IEEE*, Gulistan Raja, *Senior Member*, *IEEE*, and Thierry Bosch, *Senior Member*, *IEEE*
DOI: 10.1109/TIM.2019.2895928

***Abstract*— Correct detection of interferometric fringes is necessary to enable high resolution metric measurements using laser diode (LD) based self-mixing (SM) interferometry. For noisy, experimentally acquired SM signals, fringe detection is a challenge even when the LD remains mono-modal. This task becomes more complicated in case multiple laser modes undergo SM. In this paper, a novel SM fringe detection method is proposed which correctly processes multi-modal as well as typically encountered mono-modal SM signals. As SM fringes appear as local signal peaks in SM signals, so the proposed method uses peak detection to detect all-possible local peaks within the SM signal. Then, it successively refines its performance by removing false peaks (fringes) by analyzing corresponding SM fringe characteristics. In order to validate the proposed method for SM vibration sensing, several mono-, bi-, and tri-modal SM signals were acquired by using two different LDs normally emitting at 637 nm and 650 nm respectively. The proposed method is also tested on experimental SM signals corresponding to cases of variation in frequency as well as amplitude of remote target vibration. The proposed method has correctly detected 10786 fringes out of total 10844 fringes making up the data-set i.e. an accuracy of 99.46%. However, 55 false fringes were also detected (0.51%) while 58 true fringes were undetected (0.54%) by the proposed method.**

***Index Terms*— Vibration Measurement, Multi-modal Fringes, Fringe Detection, Self-mixing interferometry.**

I. Introduction

SELF-MIXING (SM) or optical feedback interferometry [1, 2], is being increasingly employed for measuring displacement [3, 4], distance [5, 6], velocity [7], vibration [8], flow [7], and refractive index [9] etc. providing compact, low-cost, contactless, and self-aligned instrumentation. These miniaturized and cost-effective SM laser sensors can be promising candidates for contactless displacement- and vibration-measurements required in non-destructive testing and monitoring applications, such as to ensure condition-based machine health monitoring and better preventive maintenance, for instance, by detecting bearing faults which account for approximately half of all electric machine failures [10].

Usually, SM interferometry has been performed using mono-modal laser diodes (LD). Under the assumption that only one laser mode undergoes SM then each interferometric SM fringe is considered to appear due to a remote target motion of $\lambda/2$, where λ is the wavelength of laser mode. $\lambda/2$ is thus considered the basic resolution of SM sensors. However, variation can occur in laser emission modality, during the course of sensing, resulting in bi-modal or tri-modal SM signals [11-15]. Such multi-modality has been reported for SM sensors based on in-plane semiconductor Fabry-Perot lasers [11, 12], vertical-cavity surface emitting lasers [13] and quantum cascade laser [14]. The corresponding fringe multiplicity of such multi-modal SM signals needs to be appropriately detected [16], interpreted (as each fringe now corresponds to a remote target motion of $\lambda/2m$, where m is the number of modes undergoing SM [12]), and processed to correctly retrieve the target motion. This laser modality is a function of LD's operating current [14, 15], and temperature [12] while length of external cavity can also affect the multi-modality of the SM laser sensor [11, 13]. Such multi-modality appears as a sub-periodicity within SM signal (see Fig. 1), a feature which may be used to improve the SM sensor resolution from $\lambda/2$ (mono-modal) to $\lambda/4$ (bi-modal) or $\lambda/6$ (tri-modal) [12]. However, the said higher measurement resolution associated with multi-modal SM signals cannot be achieved without correctly identifying the laser modality [16] and detecting these multi-modal SM fringes.

In typical laser applications, an optical isolator is used to prevent optical feedback (OF) into active laser cavity as OF can cause significant instability in laser operation including mode-hopping (MH) [1, 2]. However, SM interferometry is based on OF. Thus, optical isolators cannot be used within SMI set-up. Stated otherwise, MH is an inherent part of SMI especially in case of high OF [1, 2]. Consequently, guaranteed absence of MH cannot be ensured for a low-cost LD based SM sensor operating under variable conditions (in terms of reflectivity of remote target surface, and sensor-to-target distance [11, 13]). So, laser MH can always occur (causing incoherent superimposition of different individual modes [14] under SM), resulting in multi-modal SM signals. The challenge then is to correctly detect and interpret such multi-modal fringes as wrong detection or interpretation will result in drastic increase in measurement error.

DOI: 10.1109/TIM.2019.2895928

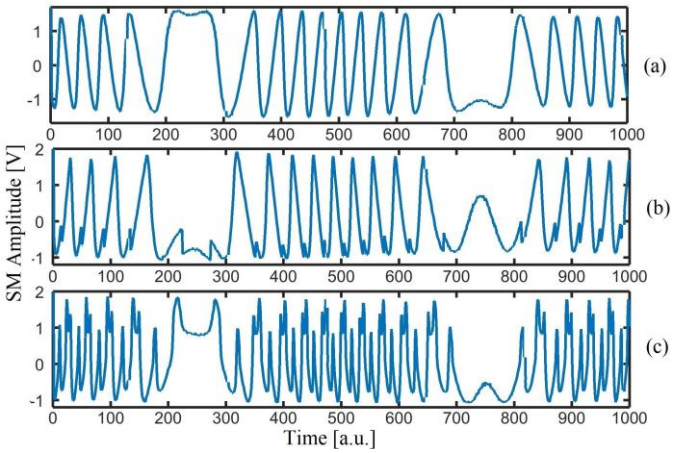

Fig. 1. Experimentally acquired self-mixing interferometric signals (a) mono-modal SM signal (b) bi-modal SM signal (c) tri-modal SM signal

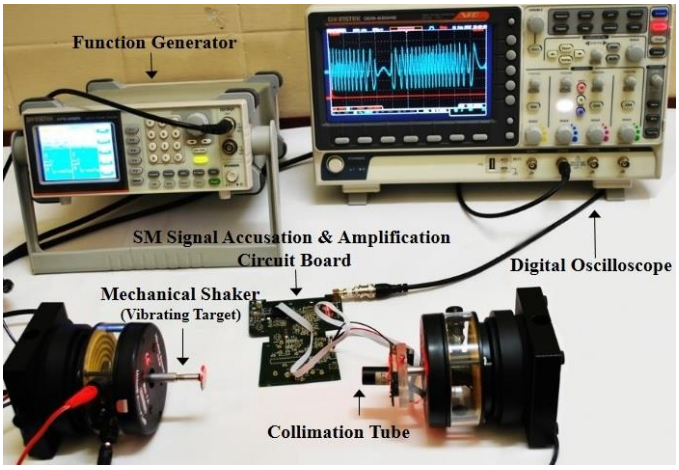

Fig. 2. Photograph of experimental set up used to acquire mono-modal, bi-modal and tri-modal SM signals corresponding to a remote vibrating target.

SM fringe detection (FD) has been a focus of recent research as it constitutes an integral part of high accuracy displacement and vibration retrieval algorithms [17-21]. Currently, various SM FD methods exist to process mono-modal SM signals. However, this task of FD becomes even more challenging in case of multi-modal SM signals in which fringes of different modes under SM exhibit different characteristics (see Fig. 1) due to incoherent superposition of constituent modes [12, 13].

For mono-modal SM signal under moderate optical feedback, SM FD can be achieved by using a comparison between the first difference of SM signal (i.e. the differentiated SM signal) and a pre-fixed threshold value [22]. In case of variation in the optical feedback (such as weak-, moderate-, or strong-feedback), different methods for FD have also been previously proposed. For example, an adaptive threshold based method [23] allowed detecting SM fringes belonging to weak-, moderate-, or strong-optical feedback based SM signals. Likewise, for weak feedback regime, SM signal fringes can be efficiently detected using the double derivative method [21] which consists in multiplying a short-duration first difference with a long-duration first difference of such a SM signal.

In case of continuous optical feedback variation (e.g. caused due to speckle phenomenon [24]), SM signal amplitude is modulated [25]. For such signals, FD has been achieved by tracking the envelope of modulated SM signal which serves as a time-varying threshold [25]. Likewise, Hilbert transform (HT) has also been used to process such SM signals as the HT based processing of analytic signal can withstand any amplitude variations [17]. Lastly, use of custom-made wavelets [26] allowed robust FD for weak-, and moderate-optical feedback based SM signals even in the presence of speckle. However, all these previous FD methods are limited only to mono-modal SM signals.

The paper is organized as follows: Section II presents SM experimental setup while proposed Multi-Modal Fringe Detection (MMFD) method is detailed in Section III. Results are presented in Section IV followed by *Discussion* and *Conclusion*.

II. SM Experimental Setup

SM occurs when a portion of laser light, illuminating the remote target, is back-scattered and re-enters the active laser cavity. Such re-injection changes the optical and spectral properties of the laser [27]. The altered optical output power (OOP), also called as the SM signal, is processed for metric measurement retrieval. OOP is detected using the built-in monitor photo-diode (PD) located at the back-facet of LD.

In order to acquire experimental mono-, and multi-modal SM signals, the experimental setup photographed in Fig. 2 has been used. A polished metallic ring (mounted on a mechanical shaker, model SF-9324 by PASCO®) was used as remote vibrating target. Sinusoidal wave of 100 Hz was applied to the shaker through a function generator (model AFG-2225 by GW Instek®). A digital storage oscilloscope (GDS-2204E by GW Instek®) was used to acquire various SM signals

Two different low-cost LDs, HL6501MG by Hitachi® and L637P5 by Oclaro® were used, one at a time, to acquire various SM signals. HL6501MG LD has threshold current (I_{th}) of 75 mA and operating wavelength (λ_0) of 650 nm providing 35 mW optical power. L637P5 LD has I_{th} of 20 mA and λ_0 of 637nm emitting 5mW optical power. Each of these LDs was housed, one at a time, in a collimation tube (model LT110P-B by Thor Labs®) having a focusing lens of 6.24 mm focal length. Adjustment of this lens allowed focusing of the emitted laser beam on to the remote vibrating target. A custom-built circuit board implements LD and PD biasing, LD current control, and SM signal acquisition and amplification.

III. Proposed Multi-Modal Fringe Detection

The proposed Multi-Modal Fringe Detection (MMFD) method is based on the idea that SM fringes can be seen as local SM signal peaks. So, a peak detection approach can be used to identify SM fringes within any mono- or multi-modal SM signal. Specifically, MMFD is based on an iterative and progressively refined use of a built-in MATLAB function called *findpeaks*. This function identifies peaks within input signal using the simple definition that a local peak is a data

DOI: 10.1109/TIM.2019.2895928

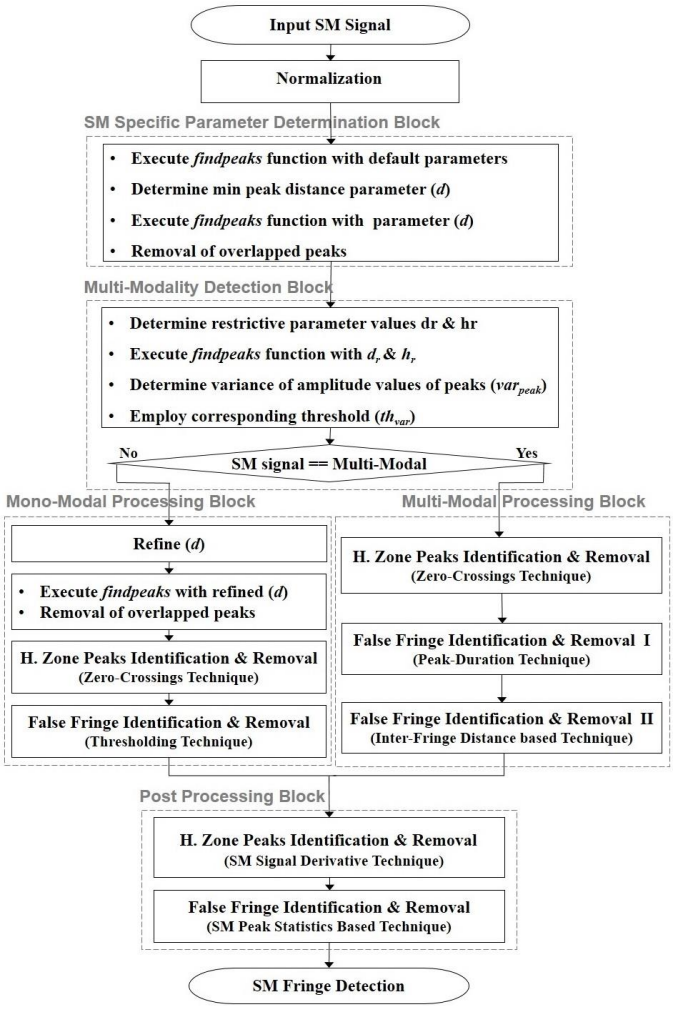

Fig 3. Schematic block diagram of proposed MMFD method.

sample that is larger than its two neighboring samples. To improve peak detection performance, it uses minimum peak distance parameter *d* which allows ignoring peaks that are very close to each other. It thus specifies a horizontal guard-band (in terms of number of samples of the input signal) so that no new peak is detected within the guard-band.

As the *findpeaks* function is a general method so it is understandable that its direct application to mono/multi-modal SM signals will not provide optimum FD results. Thus, the proposed MMFD method uses *findpeaks* in an iterative manner and then successively improves the FD performance by judiciously extracting SM signal specific information in order to update key *findpeaks* parameter. It is important to mention that, instead of processing SM signal as a whole, it is first segmented into smaller parts and then these SM signal segments are processed one by one (overlapped-segmentation approach (i.e. adjacent segments have 25% overlap to counter edge effects) is used. Care is taken so that each segment should contain at least two periods of SM signal (Fast Fourier transform (FFT) is used to provide estimate of periodicity in the input SM signal). This then ensures correct SM fringe detections even in case of change in modality of the input SM signal, and it also ensures correct processing of SM signals in case of change in frequency and peak-peak amplitude of

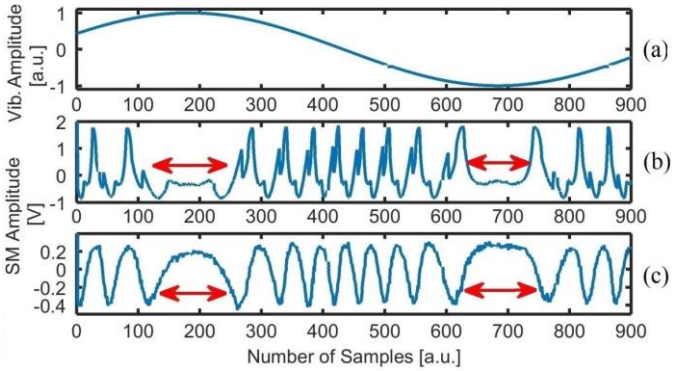

Fig. 4. Exemplar SM signals experimentally acquired by using HL6501MG laser diode emitting at wavelength (λ_0) of 650 nm: (a) the target motion (b) tri-modal SM signal and (c) mono-modal SM signal. The arrows indicate the so-called hump zones (where remote target's direction reversal occurs) of an SM signal which are zones devoid of true fringes.

remote target vibration.

Proposed MMFD method is schematically presented in Fig. 3. It can be divided into five principal blocks called as 1) SM Specific Parameter Determination Block, 2) Multi-Modality Detection Block, 3) Mono-Modal Processing Block, 4) Multi-Modal Processing Block, and 5) Post-Processing Block.

In order to graphically present important steps of the proposed method, exemplar experimental SM signals are used, shown in Fig. 4 along with target motion.

Each MMFD method block is described below.

A. SM Specific Parameter Determination Block

SM Specific Parameter Determination Block is common for both mono-modal and multi-modal SM signals. In this block *findpeaks* function is executed on SM signal segments in a one by one manner while using default parameter *d* value. As the experimental SM signals contain noise and local signal variations in addition to true fringes, a lot of false detections can hence also occur, as shown in Fig. 5.

In this work, false fringe (peak) detections are categorized into two types, namely 1) hump zone peaks (indicated by red diamonds in Fig. 5), and 2) false peaks (indicated by green circles in Fig. 5). Hump zone (denoted as H. Zone in Fig. 3)

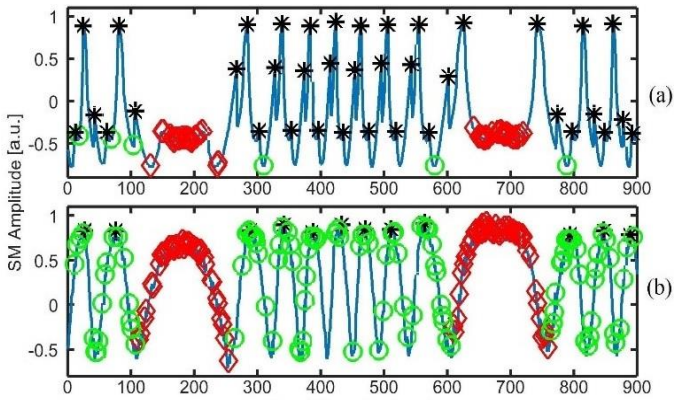

Fig. 5. Fringe detection performance with default parameter values for normalized exemplar (a) tri-modal and (b) mono-modal signals obtained from HL6501MG laser diode. Correctly detected true peaks are indicated by black stars, hump zone peaks are indicated by red diamonds, and false peaks/fringes are indicated by green circles.

DOI: 10.1109/TIM.2019.2895928

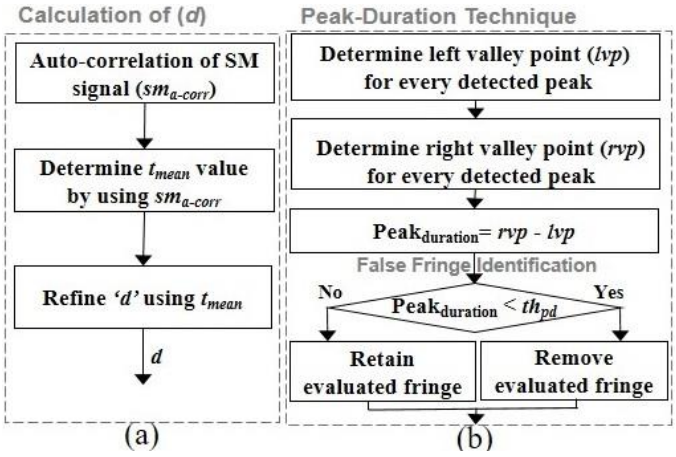

Fig. 6. (a) Flowchart of the method used to determine the value of parameter *d* (b) Flowchart of Peak-Duration Technique used for the identification of false fringes in Multi-Modal Processing block.

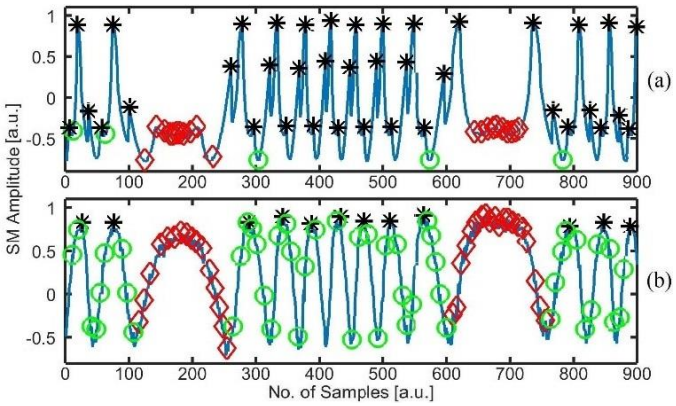

Fig. 7. Fringe detection performance with determined value of *d* parameter for exemplar (a) tri-modal and (b) mono-modal signals obtained from HL6501MG laser diode. Correctly detected true peaks are indicated by black stars, hump zone peaks are indicated by red diamonds, and false peaks/fringes are indicated by green circles.

peaks refer to those detections which occur in the so-called hump of the SM signal where target direction reversal occurs. For a vibrating remote target, hump zones thus occur at each maxima and minima of remote target vibration, and are devoid of any true fringes. Likewise, a false peak refers to any detection which cannot be associated to a true fringe e.g. it may occur due to local noise variation.

Now, in order to improve detection performance, following steps shown in Fig. 6 (a) are performed to recalculate *d* for each SM segment separately:

1) Compute auto-correlation of each SM signal segment ($sm_{a\text{-}corr}$). This allows a robust determination of any periodicity in each specific SM signal segment.

2) Any periodicity in input SM signal segment repeats as successive maxima in $sm_{a\text{-}corr}$ signal. An average of time-intervals corresponding to these maxima is computed, designated as t_{mean}, which is indicative of *d* because it is representing fringe repetition rate of the input SM signal segment under evaluation.

3) *d* is refined using a reduced value of t_{mean} (by taking 10 times smaller value of t_{mean}). A reduced value of t_{mean} is used to ensure that no true SM peak (fringe) is missed. However, a reduced t_{mean} can cause false peak (fringe) detection. As such false fringes can be removed in subsequent steps so it is important to use a reduced t_{mean} as any missed true peak (fringe) cannot be subsequently recovered.

Finally, *findpeaks* function is executed again on SM signal segments in a one by one manner with correspondingly determined value of parameter *d*. Furthermore, as overlapped-segmentation approach is used so the overlapped portions of adjacent signal segments are processed twice by *findpeaks* function. As a result, peaks in these overlapped portions are also detected twice. It is then necessary to correct these overlapped peaks by removing the doubly detected fringe. However, at the end of SM Specific Parameter Determination Block, FD performance of mono- as well as multi-modal SM signals is still not significantly improved enough, as can be observed by comparing Fig. 5 with Fig. 7.

So, in order to further improve the fringe detection performance, it is necessary to separately process mono-modal and multi-modal signals, both of which are separated by Multi-Modality Detection Block, explained below.

B. Multi-Modality Detection Block

In order to determine if the input SM signal is mono-modal or not, initial study has analyzed various parameters (such as peak to peak amplitude, variance, and zero-crossings etc.) of mono- and multi-modal SM signals. This resulted in selection of a distinguishing parameter called var_{peak} (i.e. the variance of amplitude values of input SM signal at the detected peak locations). var_{peak} is plotted in Fig. 8 showing that the variance of amplitude values of peaks of a mono-modal SM signal is always smaller than that of a multi-modal SM signal. Thus, var_{peak} is compared with a threshold th_{var} = 0.03 (corresponding to signal to noise ratio (SNR) of 12 dB for noisy mono-modal SM signals, as detailed ahead) so that mono-modal SM signals can be distinguished from multi-modal SM signals.

The four following steps are used for this purpose:

1) Use values of restrictive parameters d_r = 5*d* (here, *d* is computed for the whole SM signal by using the same approach of $sm_{a\text{-}corr}$, however, here t_{mean} is not reduced by 10 times) and h_r is minimum peak height parameter which

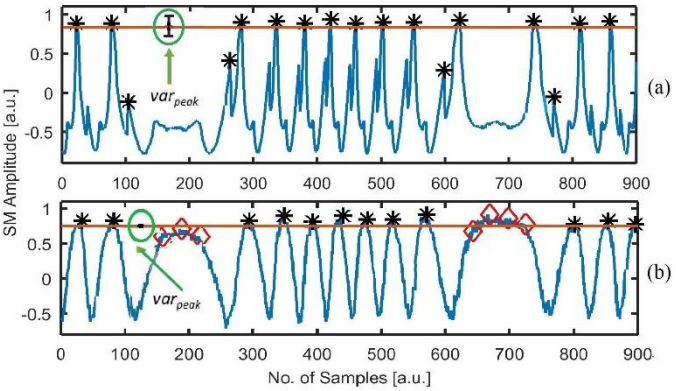

Fig. 8. (a-b) Detected peaks of exemplar SM signals with restrictive values of d_r=5*d and h_r. Horizontal red line represents mean value of amplitude of SM signal at detected peak locations while black vertical line encircled in green is representing var_{peak} value.

DOI: 10.1109/TIM.2019.2895928

corresponds to the mean of the peak amplitude values, where peaks are the peaks detected at the end of the SM Specific Parameter Determination Block.. It specifies the height of the input signal (in terms of input signal amplitude) below which no peaks are detected. Note that d_r and h_r are only used during Multi-Modality Detection Block.

2) *findpeaks* function is executed with values of d_r and h_r, resulting in detection of a small sub-set of peaks (most of which will be genuine peaks). These restrictive parameter values may eliminate multiple genuine peaks as well as false peaks. However, the objective at this stage is only to ensure that a sub-set mostly composed of genuine peaks is detected so that the variance of their peak amplitude values is not significantly affected by the inclusion of false peaks.

3) Determine var_{peak} for this sub-set of peaks.

4) An optimum variance threshold value (th_{var}) is employed, which is $th_{var} = 0.03$.

Finally, a decision about the modality of input SM signal can then be made by comparing var_{peak} with th_{var}. If $var_{peak} < th_{var}$, then input SM signal is considered mono-modal, else it is considered a multi-modal SM signal.

var_{peak} is a robust measure to identify the presence of mono-modal SM signals because for such signals, variance of amplitude values of input SM signal at the detected peak locations is zero for ideal, speckle-free, noise-less mono-modal SM signals. However, as experimental SM signals are always affected by additive noise, so th_{var} was set to 0.03 to provide robustness with respect to the noise (and possible wrong fringe detections) associated with mono-modal SM signals contained in the dataset. Simulations were carried out to quantify the noise level associated with mono-modal SM signals that would cause var_{peak}=0.03. The results indicate that additive noise corresponding to SNR of 12 dB results in var_{peak}=0.03. Thus, the proposed algorithm can correctly distinguish mono-modal SM signals with SNR $\geq$ 12 dB.

Thus at the end of Multi-Modality Detection Block, modality of input SM signal is determined which enables specific customization of *d* parameter for mono-modal or multi-modal SM signals respectively. After modality detection, the output of SM Specific Parameter Determination Block (shown in Fig. 3) is taken up and is improved in Mono- or Multi-Modal Processing Blocks, as detailed below.

C. Mono-Modal Processing Block

Mono-Modal Processing Block is composed of four sub-blocks (as shown in Fig. 3) and all of these will process the input SM signal in a piecewise manner. In the first sub-block, the value of *d* is computed for each SM segment in exactly the same manner by using $sm_{a\text{-}corr}$ as done in SM Specific Parameter Determination Block. However, here t_{mean} is reduced to half (1/2), while in former case t_{mean} was reduced by 10 times. Then, in the second sub-block, *findpeaks* function is re-executed using corresponding refined value of *d* for each SM input signal segment resulting in more accurate peak detection and reduced false fringe detections. Again, doubly detected overlapped peak pairs are corrected, by considering each of these as a single genuine peak.

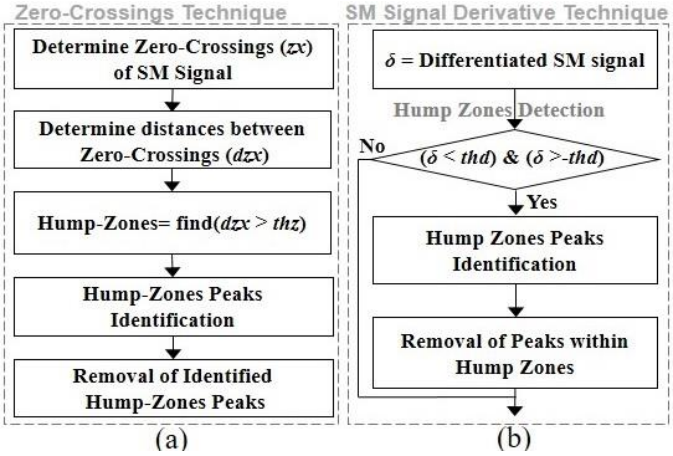

Fig. 9. (a) Flowchart of Zero-Crossings Technique which is used to identify hump zones of SM signal. (b) Flowchart of SM signal derivative Technique which is also used for the identification of hump zones.

The third sub-block performs Hump Zone Peaks Identification and Removal (shown by using diamond marker in Fig 7(b)). For this purpose, the first task is the identification of hump zones. This can be achieved by using zero-crossings of the input SM signal (see the flowchart in Fig. 9 (a)).

As can be observed in Fig. 4, distance between consecutive zero-crossings of an SM signal during a hump zone is usually greater as compared to the distance between consecutive zero-crossings occurring for true SM fringes. Thus, zero-crossings can be used for the identification of hump zones. After identification of hump zones, the false fringes detected within these hump zones are eliminated. The zero–crossings technique is also used in piecewise manner, detailed steps of zero-crossings based technique are listed below:

1) Determine zero-crossings (*zx*) of each SM signal segment separately.

2) Determine the distances (*dzx*) between consecutive *zx*.

3) Sort *dzx* in descending order.

4) Compute the time-period T_0 (reciprocal of target vibration frequency) of the SM signal segment by using FFT to estimate periodicity

5) Select top *L* number of sorted *dzx* where $L = 2*T_0$.

6) Compute average value of *L* number of selected *dzx*.

7) Multiply this average value by 1.2. The resultant value is the so-called threshold *thz* for under-process SM signal segment. The reason behind multiplying averaged *dzx* value with 1.2 is to avoid the risk of losing genuine peaks (fringes) if ever these are considered as hump zones by the above-mentioned procedure. However, this is achieved at the cost of non-detection of genuine hump zones having comparatively smaller duration. However, such unidentified hump zones can be detected at a later stage during the Post Processing Block.

8) Finally, hump zones in different SM signal segments are identified by using corresponding *thz* values. This is achieved by a simple comparison of all *dzx* with *thz*. That is, if any *dxz* > *thz*, then it is considered as indicating a hump zone.

9) After hump zone identification, all peaks within such zones are removed from original vector containing all peaks (as detected in second step of mono-modal processing block).

DOI: 10.1109/TIM.2019.2895928

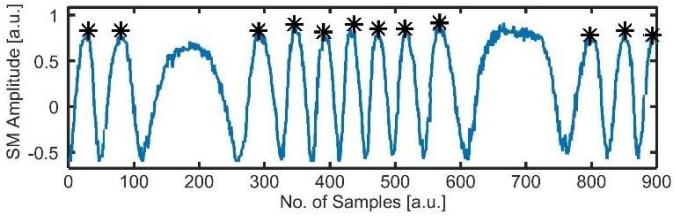

Fig. 10. Correctly detected fringes (black stars) of exemplar mono-modal SM signal after the removal of all false detections, achieved at the end of Mono-Modal Processing Block.

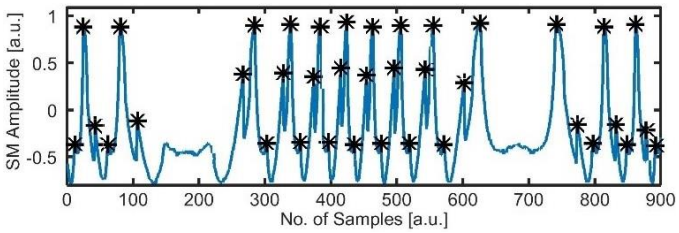

Fig. 11. True detected fringes (black stars) of exemplar multi-modal SM signal after the removal of all false detections, achieved at the end of Multi-Modal Processing Block.

Finally, the fourth sub-block performing False Fringe Identification and Removal (by using Thresholding Technique) is executed, as detailed below.

1) Identify the amplitude value which is the most common in amplitude values of peaks detected in SM signal segment.

2) Reduce this amplitude value by 50 % and use it as a threshold th_{amp} for removing false peaks (fringes) as indicated by green circles in Fig. 7(b).

3) If any detected peak's amplitude value is less than th_{amp} then it is considered as a false peak and removed.

To further remove false fringes, consecutive inter-peaks distances are determined by taking derivative of each SM segment, and then consecutive inter-peaks distances which are shorter than *d* (as computed in Refine *d* sub-block) are identified. Then, amplitude values of two peaks whose inter-peak distance is shorter than *d* are compared, and peak with smaller amplitude is removed, considering it as a false fringe. This false fringe removal procedure is done for every segment of input SM signal, using their corresponding value of *d*.

So, at the end of Mono-Modal Processing Block, FD performance has significantly improved, as seen in Fig. 10.

D. Multi-Modal Processing Block

If the input SM signal has been found to be multi-modal then Multi-Modal Processing Block is executed (see Fig. 3). In its first sub-block, Hump Zone Peaks Identification & Removal using zero-crossings techniques is executed in piecewise manner, as described previously.

Secondly, after removing hump zone peaks, steps are taken to remove false peaks (indicated by green circles in Fig. 7(a)). For this purpose, Peak-Duration Technique is used again on SM signal segment one by one (see its flowchart in Fig. 6 (b)).This technique is based on the observation that the duration of a false peak is usually much smaller than the duration of a true SM peak (fringe). This observation can then be used to remove false peaks, as per the following steps:

1) Determine the left valley point (*lvp*) of detected peak (the point from where signal starts to rise again on left side),

2) Determine the right valley point (*rvp*) of detected peak (the point from where signal starts to rise again on right side),

3) Peak duration of any detected peak can be determined by taking the difference of corresponding *lvp* and *rvp*. Durations of all peaks can be determined in a same manner.

4) Optimum peak-duration threshold (th_{pd}) parameter for each SM signal segment can be calculated by the following steps:

a) Select a portion of SM signal segment delimited by two consecutive hump zones. Do it for at least 2 portions for each segment of input SM signal.

b) Select the middle-half (50%) portion of each segment.

Thus, initial- (25%) and final- (25%) portions of each segment are discarded.

c) Peak-durations of peaks which are lying inside the selected middle half portions are selected.

d) Take median value of these selected peak-durations and set th_{pd} to half of this median value.

5) False peaks identification for each SM signal segment can then be done by using their corresponding th_{pd}. I.e., peak-durations < th_{pd} are considered as peaks and are removed.

To summarize, all peaks having smaller duration than th_{pd} are considered as false peaks. This means that th_{pd} sets the limit of the maximum measureable speed of remote target's motion given by $V_{max} = (\lambda/2m)/th_{pd}$ (where constant *m* is representing the modality of SM signal i.e. *m*=1 for mono-, *m*=2 for bi- and *m*=3 for tri-modal SM signals) [12]. E.g., in case of tri-modal exemplar SM signal segment (a zoom on portion of it shown in Fig.11), th_{pd} is fixed to 5 samples ($f_{sampling}$=100 kHz). Thus, all fringes with peak-durations <5 µs are excluded. As the employed LD has λ = 650 nm, so th_{pd}=5 fixes maximum measureable speed V_{max}=2.2 mm/s. That being said, it needs to be stated that th_{pd} is computed based only on the input SM signal. So, if an input signal is acquired for a remote target motion having a lower or higher velocity then this parameter is automatically adjusted to cater to the corresponding velocity.

So, at the end of Multi-Modal Processing Block, FD performance has also significantly improved (see Fig. 11). However, to further reduce false fringe detections, Inter-Fringe Distance based Technique is also used. It is based on inter-peak distances. Those peaks whose inter peak distance is shorter than "*d*" (as calculated in "SM Specific Parameter Determination Block") are identified and then, amplitude values of two peaks whose inter-peak distance is shorter than *d* is compared, and peak with smaller amplitude is removed, by considering it as a false fringe.

E. Post Processing Block

All hump zone peaks and false peaks have been removed from our exemplar signals at this stage. However, for many other signals in our data-set, certain hump zone peaks and false peaks still remain. So, in order to ensure their eradication, further processing is done in this Post Processing Block to address 1) hump zone peaks, and 2) false peaks.

Certain hump zones can be missed by the previously used hump-zone identification technique (based on zero-crossings technique). So, to identify these, statistics of derivative of SM signal contained within previously identified hump-zones are used to obtain an optimum threshold, called *thd*. This

DOI: 10.1109/TIM.2019.2895928

threshold is then applied on SM signal segment to identify any missed hump zone(s). Due to use to SM signal derivative, this Hump Zone Identification and Removal technique is called SM Signal Derivative technique (see its flowchart in Fig. 9(b)), and is also applied in a piecewise manner. The steps of this technique are detailed below:

1) Take derivative of each segment of input SM signal, denoted as δ.

2) Remaining hump zones can be identified by observing the variation in the amplitude of δ. As the hump zone is devoid of true fringes, so variation in δ is smaller in hump zones than in zones containing true fringes. Thus, if the amplitude values of δ are smaller than an optimum threshold (*thd*) value then the corresponding zones are identified as hump zones. *thd* for each SM signal segment is computed by the following steps:

a) Take derivative of previously identified hump zone portions (as identified by zero-crossings technique)

b) Take the absolute (mod) values of these derivative values.

c) Median value of absolute derivative values is taken as *thd* value.

3) All peaks found within such zones are again removed.

Finally, in the second and last stage of Post Processing Block, certain remaining false peaks (fringes) are identified in each SM signal segment and removed by using SM Peak Statistics Based Technique. As almost all detected peaks are true peaks at this stage of processing, so statistics of these peaks can be used to identify anomalous (false) peaks. For example, if almost all of the detected peaks are located in the upper-half of input SM signal segment then any peak (fringe) detected in the lower-half of input SM signal segment can be considered as a false peak. This is achieved in the proposed method by finding out the SM amplitude value associated with every detected peak. Then, if the number of negative-amplitude associated peaks is far less than the number of positive-amplitude associated peaks, then these negative-amplitude associated peaks are considered anomalous (i.e. false peaks) and are removed.

IV. Results

Correct FD results are graphically shown for different SM signals of mono-, bi-, and tri-modal experimental SM signals. It may be seen that the number of fringes per period is different for each of these signals due to different peak to peak

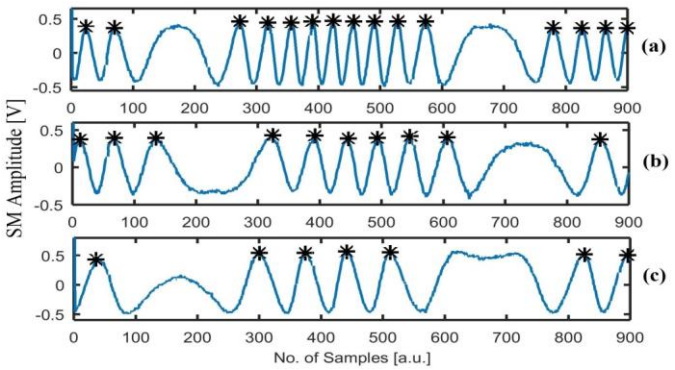

Fig. 12. (a-c) Detected true peaks (fringes), indicated by black stars, of three different correctly processed experimental mono-modal SM signals.

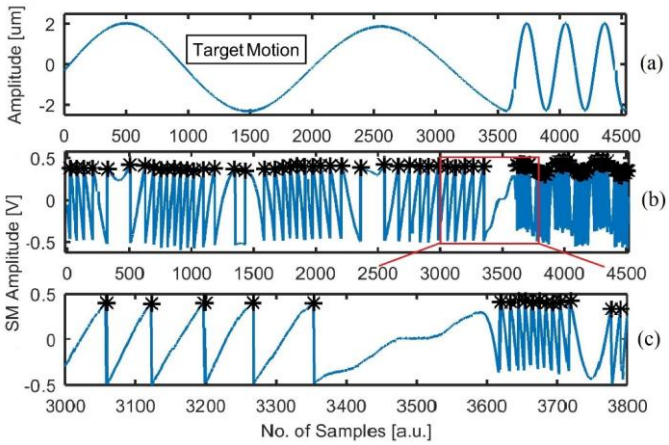

Fig.13. Fringe detection of SM signal corresponding to sudden change in target's frequency (as caused by sudden acceleration of remote target): (a) reference target motion, (b) correctly processed corresponding SM signal, and (c) zoom on portion of part (b) indicated with red rectangle.

amplitude of remote target. This shows that the proposed MMFD method is effective even in case of variation in target's amplitude. It may also be mentioned that each SM signal acquisition contains 100 periods but only about one period each is shown below for the sake of clarity.

A. Mono-Modal SM Signals

Performance of proposed MMFD method for three (out of total 22) different mono-modal SM signals is graphically presented in Fig. 12.

Note that due to use of SM signal segmentation approach, the proposed MMFD method is also able to process such SM signals corresponding to sudden variation in frequency of remote target vibration (such as caused by sudden acceleration of target vibration). One such SM signal along with reference target motion is shown in Fig. 13.

B. Bi-Modal SM Signals

Performance of proposed MMFD method for three (out of total 20) bi-modal SM signals is graphically shown in Fig. 14.

C. Tri-Modal SM Signals

Performance of proposed method for three (out of total 22) different tri-modal SM signals in seen in Fig. 15.

Correct processing of a tri-modal SM signal corresponding to sudden variation in frequency of target vibration is also

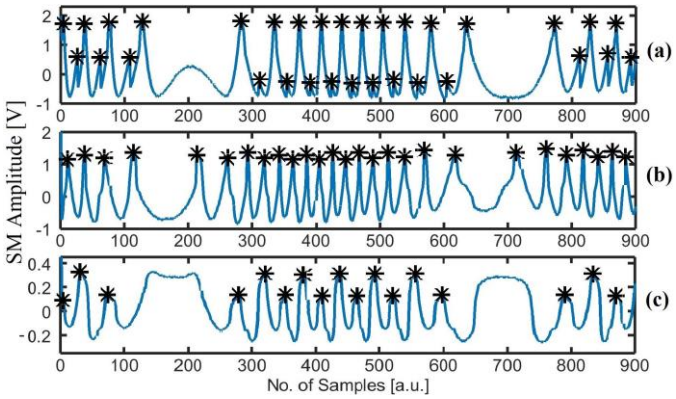

Fig. 14. (a-c) Detected true peaks (black stars) of three different correctly processed experimental bi-modal SM signals.

DOI: 10.1109/TIM.2019.2895928

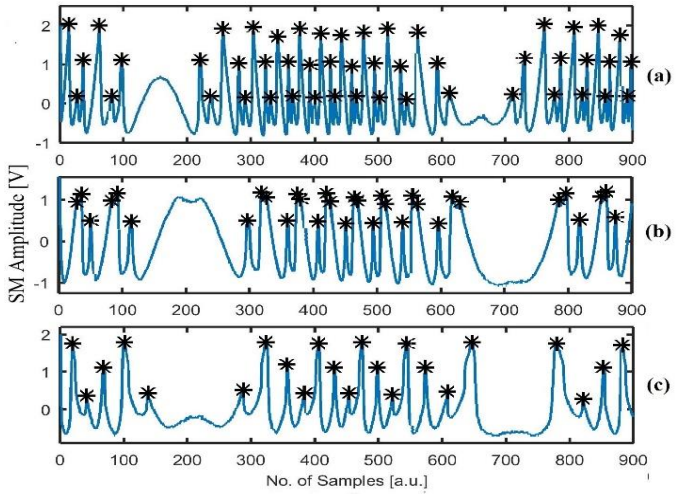

Fig. 15. (a-c) Detected true peaks (black stars) of three different correctly processed tri-modal SM signals.

presented in Fig. 16.

D. Data-set Results

The proposed MMFD method was tested by using a data-set of 66 experimental SM signals comprising 22 signals each for mono-, bi-, and tri-modal SM signals. Cumulative results, in terms of total number of fringes (N_F), total number of true fringe detections (N_{TF}), and total number of false fringe detections (N_{FF}), ratio of true fringe detections to total fringes $R_{TF} = (N_{TF}/N_F) \times 100$, ratio of false fringe detections to total fringes $R_{FF} = (N_{FF}/N_F) \times 100$, and ratio of undetected fringes to total fringes $R_{UF} = (N_F - N_{TF}/N_F) \times 100$ are presented in Table I.

TABLE I
FRINGE DETECTION PERFORMANCE RESULTS USING THE COMPLETE DATA-SET OF MONO-, BI-, AND TRI-MODAL SM SIGNALS

Mode	Dataset	N_F	N_{TF}	N_{FF}	R_{TF} (%)	R_{FF} (%)	R_{UF} (%)
Mono	22	1515	1513	4	99.86	0.26	0.13
Bi	22	3640	3611	21	99.20	0.57	0.79
Tri	22	5689	5662	30	99.52	0.52	0.47
Total	66	10844	10786	55	99.46	0.51	0.54

V. DISCUSSION

As seen in Table I, after applying MMFD, certain true SM fringes remain undetected (0.54 % for the data-set). One such case is shown in Fig. 17 where all fringes are correctly detected except one, as highlighted with a red diamond.

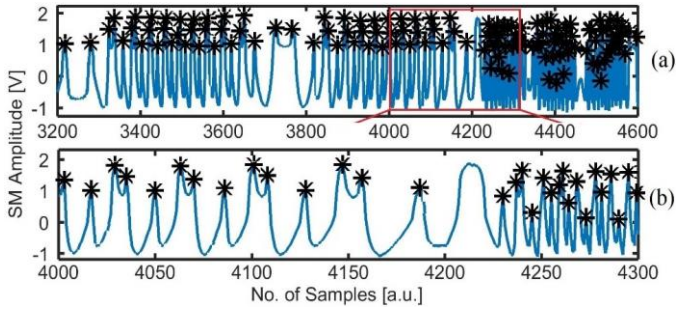

Fig.16. Fringe detection of multi-modal SM signal corresponding to sudden change in target's frequency: (a) correctly processed multi-modal SM signal, (b) zoom on portion indicated by red rectangle in (a).

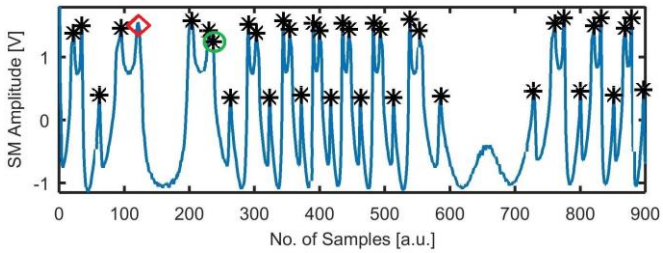

Fig. 17. Tri-modal SM signal in which all true fringes were correctly detected (marked by black stars) except for one true fringe which was missed, as marked by red diamond. Likewise, one false fringe was also detected, as marked by green circle.

Interestingly, this fringe was detected during initial steps of MMFD. However, during Post Processing stage, this fringe was removed as it came within an identified hump. This happened due to actual shorter duration of the corresponding hump zone (note that the other hump zone in Fig. 17 has longer duration). Such omission of true fringes can be improved by devising a better hump zone identification technique so that all identified hump zones do not encroach upon true SM fringes.

Likewise, MMFD is currently unable to eliminate certain false fringes (0.51 % for the data-set). One such case is shown in Fig. 17, highlighted with green circle. In fact, these false fringes are hump zone peaks which could not be removed completely. There are two reasons behind non-removal of such a false fringe. First, the width of such a false fringe happened to be comparable to the widths of true fringes contained within the same SM signal. As a result, such a false fringe could not be eliminated by the Peak-Duration Technique. Second, the SM signal amplitude associated with such a false fringe happened to be comparable to the SM signal amplitude associated with almost all other truly detected fringes. As a result, such a false fringe could also not be eliminated by the SM Peak Statistics Based Technique.

Finally, the effect of multimodality in the SM signal is usually observed up to three modes [10-13]. For the present work also, only up to three modes were observed for the employed laser diodes. The proposed algorithm, however, is able to distinguish mono-modal SM signals from the multi-modal SM signals. Note that the proposed algorithm's primary task is to detect all fringes present within any given input SM signal. Thus, it is not restricted to just three modes and could be extended to correctly process the fringes contained in such SM signals in which more than three modes contribute individual sets of interferometric fringes to the SM signal.

VI. CONCLUSION

Fringe detection is a fundamental part of SM signal processing algorithms, designed for the retrieval of remote target's displacement and vibration measurements. The proposed method is based on detection of peaks within the input SM signal followed by successive refinement of key peak detection parameters as well as removal of falsely detected peaks. Thus, the novelty of proposed method is its capability of robust fringe detection of multi-modal (bi-modal and tri-modal) SM signals along with traditionally

DOI: 10.1109/TIM.2019.2895928

encountered mono-modal SM signals. This proposed method has been successfully tested on experimental mono-modal, bi-modal and tri-modal SM signals (acquired using two different LDs, one at a time, normally emitting at 637nm and 650 nm respectively) with an accuracy of 99.46%. It is also able to correctly process SM signals corresponding to cases where changes occur in frequency and peak-peak amplitude of remote target vibration.

Future work will focus on further improvement in fringe detection as well as real-time hardware implementation of the proposed method so that mono- and multi-modal SM signals can be detected in real-time.

REFERENCES

[1] T. Taimre, M. Nikolić, K. Bertling, Y. L. Lim, T. Bosch, and A. D. Rakić, "Laser feedback interferometry: A tutorial on the self-mixing effect for coherent sensing," *Adv. Opt. Photon.*, vol. 7, pp. 570-631, 2015.

[2] S. Donati, "Developing self-mixing interferometry for instrumentation and measurements," *Laser Photon. Rev.*, vol. 6, pp. 393-417, 2012.

[3] I. Milesi, M. Norgia, P. P. Pompilio, C. Svelto, and R. L. Dellaca, "Measurement of local chest wall displacement by a custom self-mixing laser interferometer," *IEEE Trans. Instrum. Meas.*, vol. 60, pp. 2894-2901, 2011.

[4] A. G. Demir, P. Colombo, M. Norgia, and B. Previtali, "Evaluation of self-mixing Interferometry performance in the measurement of ablation depth," *IEEE Trans. Instrum. Meas.*, vol. 65, pp. 2621-2630, 2016.

[5] M. Norgia, G. Giuliani, and S. Donati, "Absolute distance measurement with improved accuracy using laser diode self-mixing interferometry in a closed loop," *IEEE Trans. Instrum. Meas.*, vol. 56, pp. 1894-1900, 2007.

[6] A. Magnani, A. Pesatori, and M. Norgia, "Real-time self-mixing interferometer for long distances," *IEEE Trans. Instrum. Meas.*, vol. 63, pp. 1804-1809, 2014.

[7] I. Ohno and S. Shinohara, "A comparative study for the assessment on blood flow measurement using self-mixing laser speckle interferometer," *IEEE Trans. Instrum. Meas.*, vol. 57, pp. 355-363, 2008.

[8] Z. A. Khan, U. Zabit, O. D. Bernal, M. O. Ullah, and T. Bosch, "Adaptive Cancellation of Parasitic Vibrations Affecting a Self-Mixing Interferometric Laser Sensor," *IEEE Trans. Instrum. Meas.*, vol. 66, pp. 332-339, 2017.

[9] Y. Zhang, Y. Wei, C. Chen, W. Huang, X. Wang, and H. Xu, "Self-Mixing Interferometer Based on Frequency Analysis Method for Accurate Refractive Index Measurement," *IEEE Photon. J.*, vol. 8, pp. 1-6, 2016.

[10] W. Zhou, T. G. Habetler, and R. G. Harley, "Bearing condition monitoring methods for electric machines: A general review," in *Diagnostics for Electric Machines, Power Electronics and Drives, 2007. SDEMPED 2007. IEEE Inter. Symp. on*, 2007, pp. 3-6.

[11] L. Lv, H. Gui, J. Xie, T. Zhao, X. Chen, A. Wang, *et al.*, "Effect of external cavity length on self-mixing signals in a multilongitudinal-mode Fabry–Perot laser diode," *Appl. Opt.*, vol. 44, pp. 568-571, 2005.

[12] M. Ruiz-Llata and H. Lamela, "Self-mixing technique for vibration measurements in a laser diode with multiple modes created by optical feedback," *Appl. Opt.*, vol. 48, pp. 2915-2923, 2009.

[13] J. R. Tucker, A. D. Rakić, C. J. O'Brien, and A. V. Zvyagin, "Effect of multiple transverse modes in self-mixing sensors based on vertical-cavity surface-emitting lasers," *Appl. Opt.*, vol. 46, pp. 611-619, 2007/02/01 2007.

[14] J. Keeley, J. Freeman, K. Bertling, Y. L. Lim, R. A. Mohandas, T. Taimre, *et al.*, "Measurement of the emission spectrum of a semiconductor laser using laser-feedback interferometry," *Sci. Rep.*, vol. 7, p. 7236, 2017.

[15] T. Pham, H. Seat, O. Bernal, F. Surre, and T. Bosch, "Self-mixing sensing under strong feedback using multimode semiconductor lasers," in *Lasers and Electro-Optics Pacific Rim (CLEO-PR), 2013 Conference on*, 2013, pp. 1-2.

[16] U. Zabit, K. Shaheen, M. Naveed, O. D. Bernal, and T. Bosch, "Automatic Detection of Multi-modality in Self-Mixing Interferometer," *IEEE Sensors J.*, 2018.

[17] A. L. Arriaga, F. Bony, and T. Bosch, "Real-time algorithm for versatile displacement sensors based on self-mixing interferometry," *IEEE Sensors J.*, vol. 16, pp. 195-202, 2016.

[18] O. D. Bernal, U. Zabit, and T. Bosch, "Study of laser feedback phase under self-mixing leading to improved phase unwrapping for vibration sensing," *IEEE Sensors J.*, vol. 13, pp. 4962-4971, 2013.

[19] A. Ehtesham, U. Zabit, O. Bernal, G. Raja, and T. Bosch, "Analysis and Implementation of a Direct Phase Unwrapping Method for Displacement Measurement using Self-Mixing Interferometry," *IEEE Sensors J.*, vol. 17, pp. 7425-7432, 2017.

[20] Y. Fan, Y. Yu, J. Xi, and J. F. Chicharo, "Improving the measurement performance for a self-mixing interferometry-based displacement sensing system," *Appl. Opt.*, vol. 50, pp. 5064-5072, 2011.

[21] Z. Wei, W. Huang, J. Zhang, X. Wang, H. Zhu, T. An, *et al.*, "Obtaining Scalable Fringe Precision in Self-Mixing Interference Using an Even-Power Fast Algorithm," *IEEE Photon. J.*, vol. 9, pp. 1-11, 2017.

[22] C. Bes, G. Plantier, and T. Bosch, "Displacement measurements using a self-mixing laser diode under moderate feedback," *IEEE Trans. Instrum. Meas.*, vol. 55, pp. 1101-1105, 2006.

[23] U. Zabit, T. Bosch, and F. Bony, "Adaptive transition detection algorithm for a self-mixing displacement sensor," *IEEE Sensors J.*, vol. 9, pp. 1879-1886, 2009.

[24] S. Donati, G. Martini, and T. Tambosso, "Speckle pattern errors in self-mixing interferometry," *IEEE J. Quantum Electron.*, vol. 49, pp. 798-806, 2013.

[25] A. A. Siddiqui, U. Zabit, O. D. Bernal, G. Raja, and T. Bosch, "All Analog Processing of Speckle Affected Self-Mixing Interferometric Signals," *IEEE Sensors J.*, vol. 17, pp. 5892-5899, 2017.

[26] O. Bernal, H. C. Seat, U. Zabit, F. Surre, and T. Bosch, "Robust Detection of Non Regular Interferometric Fringes from a Self-Mixing Displacement Sensor using Bi-Wavelet Transform," *IEEE Sensors J.*, vol. 16, p. 7903, 2016.

[27] R. Lang and K. Kobayashi, "External optical feedback effects on semiconductor injection laser properties," *IEEE J. Quantum Electron.*, vol. 16, pp. 347-355, 1980.

Muhammad Usman received the M.Sc. degree in electrical engineering from the University of Engineering & Technology, Taxila, Pakistan, where he was a full time Research Scholar from 2016 to 2018. His research interest is in self-mixing interferometry-based algorithm design.

Usman Zabit (M'12) received the Ph.D. degree from the Institut National Polytechnique Toulouse (INPT), France, in 2010. He held a post-doctoral position with LAAS-CNRS, France, until 2012. He is currently an Associate Professor with the National University of Sciences and Technology, Islamabad, Pakistan.

Olivier D. Bernal (M'03) received the M.Sc. degree in electrical engineering and the Ph.D. degree from the Institut National Polytechnique Toulouse (INPT), France, in 2003 and 2006, respectively. He joined the Laboratory of Optoelectonics and Embedded Systems, LAAS-CNRS and INPT in 2009, where he is currently an Assistant Professor. His main research interests are in analog circuit design for optoelectronics and space applications.

Gulistan Raja (SM'14) received the master's degree in information systems engineering from Osaka University in 2002 and the Ph.D. degree in electrical engineering from University of Engineering & Technology (UET), Taxila, Pakistan in 2008. He is currently a Professor in the Electrical Engineering Department, UET, Taxila, Pakistan.

Thierry Bosch (M'93–SM'06) is a Professor with the Institut National Polytechnique Toulouse, ENSEEIHT, and the Head of the Optoelectronics for Embedded Systems Research Group, LAAS-CNRS. His research interests include laser industrial instrumentation development, including range finding techniques, vibration and velocity measurements.

DOI: 10.1109/TIM.2019.2895928